Structural investigation of composite phases Ba1+x[(NaxMn1–x)O3] with x= 2/7, 5/17 and 1/3 ; exotic Mn4.5+ valence in perovskite-like structure

Pascal Roussel, Olivier Perez, Eric Quarez, Henri Leligny, Olivier Mentré

Zeitschrift fr Kristallographie

Structural investigation of composite phases $Ba_{1+x}[(Na_xMn_{1-x})O_3]$ with x$\simeq$ 2/7, 5/17 and 1/3 ; exotic Mn$^{4.5+}$ valence in perovskite-like structure

Dr Pascal Roussel: Laboratoire LCPS (CNRS UMR 8012), Ecole Nationale Superieure de Chimie de Lille Bat C7a - BP 90108, 59652 Villeneuve d'Ascq , France
Tel: (+33) (0)3 20 33 64 34, Fax: (+33) (0)3 20 43 68 14, E-Mail: pascal.roussel@ensc-lille.fr
A quintal of boneless meat

Dr Olivier Pérez: Laboratoire CRISMAT/ENSICAEN (CNRS UMR 6508), Bd du Maréchal Juin, 6, 14050 Caen , France
Tel: (+33) (0)2 31 45 26 13, Fax: (+33) (0)2 31 95 16 00, E-Mail: olivier.perez@ensicaen.fr
Half quintal of meatless bones

Dr Eric Quarez: Laboratoire LCPS (CNRS UMR 8012), Ecole Nationale Superieure de Chimie de Lille Bat C7a - BP 90108, 59652 Villeneuve d'Ascq , France
Fax: (+33) (0)3 20 43 68 14,

Dr Henri Leligny: Laboratoire CRISMAT/ENSICAEN (CNRS UMR 6508), Bd du Maréchal Juin, 6, 14050 Caen , France
Tel: (+33) (0)2 31 45 26 13, Fax: (+33) (0)2 31 95 16 00,
I am not inside !

Dr Olivier Mentré: Laboratoire LCPS (CNRS UMR 8012), Ecole Nationale Superieure de Chimie de Lille Bat C7a - BP 90108, 59652 Villeneuve d'Ascq , France
Fax: (+33) (0)3 20 43 68 14, E-Mail: olivier.mentre@ensc-lille.fr

Keywords: hexagonal perovskite, composite structure, modulation, X-ray, single crystal, manganite

MS-ID: Heft: / ()	pascal.roussel@ensc-lille.fr	March 9, 2005

Abstract

Structural models are proposed for three composite compounds of chemical formula $Ba_{1+x}[(Na_xMn_{1-x})O_3]$ (x$\simeq$2/7, 5/17 and 1/3) by single crystal X-ray diffraction ; super space formalism is used to obtain an unified description of the three phases. The $[(Na_xMn_{1-x})O_3]$ framework is built up from the stacking of face sharing MnO_6 octahedra and NaO_6 trigonal prisms. The displacive modulations relating to these metallic columns were particularly difficult to modelize. Thus a model, including both discontinuous crenel-like functions for Ba atoms and continuous atomic strings for the Mn/Na sites has finally been retained. The large displacement of the oxygen atoms ($\simeq \pm 0.7$ Å) in comparison with that observed for related compounds ($\simeq \pm 0.3$ Å) makes it a direct consequence of the Na^+ alkali insertion inside the trigonal prisms. Owing to this insertion, the Mn atoms exhibit, in the three phases, an "exotic" oxidation state of about + 4.5.

1 Introduction

These last years, several studies were devoted to the compounds of general formula $A_{1+x}(A'_xB_{1-x})O_3$ particularly for their promising electronic and magnetic properties [1, 2, 3, 4, 5, 6, 7, 8, 9, 10, 11, 12, 13]. Their structures, of trigonal symmetry, are related to the 2H hexagonal perovskite framework (see ref. [14]). They are built up from metallic columns running along the ternary axis direction and delimiting channels where the A divalent cations (Ca, Sr or Ba usually) take place. The metallic columns are formed from the stacking of face sharing octahedra (O) and trigonal prisms (P) occupied by the B transition metal and the A' (of various nature) respectively. The valences of B-A' pairs in such systems adjust to the cationic natures and to the x value, *e*.g. note the Ru^{5+} state in $Sr_{1.33}(\square_{0.33}Ru_{0.66})O_3$ where prisms are empty [15]. Various sequences of the O and P polyhedra (see ref. [16] for review) may be observed giving rise, in most of the cases, to large periods (or pseudo periods) along the ternary axis direction [001]. The first structural studies were described using supercells and standard 3D space groups (SG) symmetry [2, 15, 17, 18]. Moreover, for very large **c** periods, the 3D treatment induces strong correlations between the different refined parameters preventing a reliable structure determination. Furthermore, several SG were found to describe the different structures, preventing to give an unified vision for it. Some authors [12, 19, 20, 21, 22, 23, 24, 25, 26] used the 4D approach to solve these problems. A theoretical work was also undertaken by other authors [22] to give an unified description of this family ; thus, these compounds can be considered as composite crystals with two interpenetrating sublattices, a rhombohedral one ($A'_xB_{1-x}O_3$ atomic part) and an hexagonal one (A_{1+x} atomic part) exhibiting, in the general case, incommensurate **c** periodicities. This composite approach make it possible to describe the structure of all the family using an unique pair of superspace group (SSG), *i*.e. a same 4D symmetry. This composite approach is also interesting owing to the important decrease of the number of parameters to be refined in comparison with the 3D classical treatment. Strong displacive modulations are observed for all crystals of the $A_{1+x}(A'_xB_{1-x})O_3$ family. This behaviour appears rather different from this observed in the majority of composite crystals where the interactions between the two subsystems are usually weak and then give rise to small displacive modulation.

An interesting feature concerns the ratio $\gamma = \frac{c_1}{c_2}$ of the **c** parameters of the two component lattices which can be written as a function of x, *i*.e to the chemical formula. Denoting D_O and D_P the heights of the octahedra and the trigonal prisms along [001] and assuming the Ba atoms are located in the two types of atomic planes $[Ba_3NaO_6]$ and $[Ba_3O_9]$, it is possible to calculate c_1 and c_2. It is obvious that $c_1 = xD_P + (1-x)D_O$ while c_2 can be calculated averaging the three types of expected Ba-Ba distances $D_O+D_P/2$, D_P and $2D_O$ which occur with the frequencies x/X, $x/2X$ and $(1-2x)/2X$ ($X = x+x/2+(1-2x)/2$). This leads to $c_2 = \frac{x\times D_P+(1-x)D_O}{(1+x)/2}$ and then to $\gamma = \frac{1+x}{2}$ (this calculation is explained in detail elsewhere [27]) ; note that γ is independant of the D_P/D_O ratio. Moreover, this result explains well the general formula given for the phases since the γ ratio is related to the stoichiometry.

Recently the crystal structure of the x =1/3 term of the $Ba_{1+x}(Na_xMn_{1-x})O_3$ using a standard 3D model because of strong evidences of its commensurate nature [27] was published. We report here an unified structural study of three different compounds within these series (x $\simeq$ 2/7, 5/17 and 1/3) using the 4D superspace formalism. In these compounds, the Na^+ cationic nature in A' sites lead to a formal valence closed to +4.5 for manganese.

2 Experiment, Data collection and Symmetry

Single crystals of $Ba_{1+x}Na_xMn_{1-x}O_3$ were grown by electrosynthesis using the electrochemical system and conditions previously described [27]. An EDS (energy dispersive spectroscopy) analysis was performed on the selected single crystals and confirmed the only presence of barium, sodium and manganese. One must also notice that the electrosynthesis permitting this preparation is hardly reproducible. Moreover, none of the numerous attempts performed to prepare the title compounds by solid state reaction under different experimental conditions such as heating in air, flowing N_2, or $NaOH$ flux from $BaCO_3$/ $Ba(OH)_2 - 3H_2O$, $MnO_2/Mn_2O_3, Na_2CO_3$ lead to the expected materials.

Preliminary studies were undertaken for the three single crystals on a three circles Bruker SMART CCD 1K, leading to the γ values determination (2/3, 9/14 and 11/17). Then the ideal 3D models, *i*.e. the O/P sequences have been predicted help to previous theoretical investigations [22] as intensively

detailed in our prior work [27], and roughly refined [28]. In a second stage, in order to ensure the commensurate character or not of the concerned samples and for a more accurate data collection, supplementary studies were performed on a Nonius KappaCCD diffractometer. The main investigation strategy is detailed as follows :

Frames were collected with a classical "phi-omega scans" strategy for $0 \leq \theta \leq 30^\circ$ with a small scan angle (0.3° / frame) and a short sample-detector distance (Dx=34 mm). The precession pictures calculated from these series of frames are enough precise to obtain an overall view of the reciprocal space.

The X-ray diffraction patterns showed the existence of two sets of main spots, one characteristic of a rhombohedral lattice refering to the $(Na_xMn_{1-x})O_3$ structural part, the other, with stronger spots, typical of an hexagonal lattice relating to the Ba_{1+x} structural part suggesting a composite description to be chosen. Satellite reflections with significant intensities, resulting from strong modulation inside the two composite subsystems, were observed up to the second order. The c hexagonal unit cell parameters of the $(Na_xMn_{1+x})O_3$ and Ba_{1+x} sublattices are noted c_1 and c_2 respectively. The modulation wave vectors of the two composite parts are then defined from $q_1^* = c_2^* = \gamma c_1^*$ and $q_2^* = c_1^* = \gamma^{-1} c_2^*$ with $\gamma = \frac{c_1}{c_2}$. For such compounds, this γ ratio is related to the chemical composition and given by $\gamma = (1+x)/2$. The cell parameters of each subsystem are given in Table 1. Note that, except for the crystal exhibiting the shortest periodicity (x=1/3) where satellite reflections show a full overlapp, it was not possible to conclude on the commensurate or incommensurate character of the modulation. The unit cell parameters of the two lattices, indeed, cannot be measured with an enough accuracy to know if the γ ratio is really rational or irrational. Consequently, for all crystals, a supercell can also be used to describe the diffraction pattern. These supercells are summarized in Table 1.

Systematic twins, generated by a two fold axis parallel to the ternary axis (yielding the common obverse/reverse twinning law), were evidenced from the supplementary spots appearing on the l≠3n reciprocal levels of the rhombohedral lattice and where taken into account in the subsequent refinements.

This first diffraction experiment was also very helpfull to determine a suitable strategy for the final data collection. Let us outline that the three crystals exhibit large and diffuse diffraction spots. A strategy based on "phi-omega scans" has been chosen. According to the c parameter of the supercells, the scan angle and the Dx value were adjusted to limit the overlapping of reflections, $i.e.$ for the crystal with $c \simeq$46 Å the scan angle and the Dx parameter were fixed respectively to 0.3°/frame and 70 mm. The diffracted intensities were collected up to $\theta = 45^\circ$. A redundancy of 2 for 90% of the reflections was chosen. To measure the weakest reflections, mainly the second order satellite reflections, and to avoid problem due to detector saturation, frames were collected both with large (180 s/°) and small (18 s/°) exposure times ; they were merged and rescaled afterwards.

The EvalCCD software [29] was used to extract reflections from the collected frames (more than 4500 frames for the crystal with x=5/17) within the supercell description. Data were corrected from absorption using Jana2000 program [30] within the analytical option based on the crystal morphology. The diffraction pattern is consistent with a trigonal symmetry.

As mentioned above, a composite description can be adopted. The whole reflections are then indexed using four integers hklm where hkl0 and hk0m denoting the main reflections of the first and second composite parts respectively. The observed conditions, limiting the possible reflections, hklm : -h+k+l=3n and h0lm : m=2n are consistent with the super space groups pairs $R\overline{3}m(00\gamma)0s$: $P\overline{3}c1(00\gamma^{-1})$ and $R3m(00\gamma)0s$: $P3c1(00\gamma^{-1})$ and where the γ and γ^{-1} wave vector choice denotes the subsystem 1 or the subsystem 2 as the reference lattice.

The interest of such a composite approach for commensurate or quasi commensurate structures is double : firstly it allows us to give a common description for different members of a same family and secondly it induces a reduction of the number of parameters thanks to 4D symmetry restrictions. Thus, classical 3D refinement requires the introduction of 382 atomic parameters versus 72 in the 4D approach !!

Within the commensurate hypothesis, the 3D symmetry of the superstructure can be derived from the 4D SSG as detailed elsewhere [22]; the different possible space groups, listed in Table 1, are found from the sets of particular 3D sections of the 4D space. These section are defined from the internal t parameter ($t = \overline{x}_4 - q^* < r >$) where $\overline{x}_4$ is a coordinate along the internal space and $< r >$ an average position in physical space.

3 Structure refinement

As explained above, the studied compounds can be describe using either a supercell or a composite approach. Nevertheless, in this article, the 4D description, allowing the unification by a same model of the three phases, will be more detailed.

3.1 classical 3D approach

As reported elsewhere [27], the structure of $Ba_{1+x}[(Na_xMn_{1-x})O_3]$ with x=1/3 has been successfully refined in the P321 SG. The reasonable thermal parameters values assorted with the final R = 3.21 % comfort the validity of the commensurate γ= 2/3 approximation, even if thermal displacement parameters along the [001] direction for some Mn atoms may suggest the existence of a slight static disorder over the column cations. As a matter of fact, this could also denotes a positional relaxation of Na/Mn cations in this particular structural kind, confined within a small commensurate period, or more probably a tiny deviation from the x = 1/3 rational value.

The structure of $Ba_{1+x}[(Na_xMn_{1-x})O_3]$ with x=2/7, in spite of large value of the c parameter in the 3D approach, can be classicaly studied owing to the high symmetry of the crystal (S.G.: $R\overline{3}c$); the number of refinement parameters is indeed relatively small (inferior to 90).

3.2 4D approach

Models for the structures were searched for and refined using the program Jana2000 [30] considering centrosymmetric SSG. Crystals with γ=9/14 and γ=11/17 exhibit large periods along [001] in the supercell description ; overlapping of main and satellite reflections (only observed up to the second order) are unlikely. Consequently, incommensurate modulation, making possible a stable refinement of discontinuous modulation functions, was assumed. As already mentioned, for the $\gamma = 1/3$ commensurate case, the two possible sections were tested ; the best refinement result was obtained for the section t=1/36 corresponding to the P32 symmetry.

3.2.1 The Ba_{1+x} sublattice

As expected, the modulation of Ba is likely the main one allowing the strongest satellite reflections to be explained. Two different models were attempted for this Ba species, the first with only one atom and an harmonic modulation, and the second model with two different atoms described by crenel functions.

model A : a continuous modulation Within this model, a continuous transversal modulation (displacement $U(\overline{x}_{4,2}) \perp q_2^*$) was assumed, the Ba atom occupying in the average structure the special position (1/3 0 1/4) of 32 point symmetry. The displacement $U(\overline{x}_{4,2})$ is then strongly constrained owing to the high symmetry $\begin{pmatrix} 3 & \frac{2}{1} \\ t & \end{pmatrix}$ of the atomic string in 4D space. The internal parameter $\overline{x}_{4,2}$ is defined as $\overline{x}_{4,2} = \gamma^{-1} < z_{Ba} > +n_3\gamma^{-1}$, where the n_3 integer specifies the unit cell along c_2. t means a τ shift of 2/3 in the internal space.

model B : a discontinuous modulation A discontinuous transversal modulation was also considered for the Ba atom ; this model used in a great number of previous related works (for details see [31, 32, 21]), assumes two types of Ba atoms, Ba(1) and Ba(2), related to the two kinds of layers, with the position $(1/3 - \Delta x_1\ 0\ 1/4)$ and $(1/3 + \Delta x_2\ 0\ 1/4)$ in the average structure rather than the (1/3 0 1/4) position ($\Delta x_1\ ,\ \Delta x_2\ > 0$). The 3D symmetry of the site is then reduced to 2_x. The occupancy of these two sites is described with crenel functions centred at $\overline{x}_{4,2}$ =1/2 and 0 respectively and with $\overline{x}_{4,2}$ intervals Δ_1 and Δ_2 refering to the partial Ba(1) and Ba(2) populations respectively ; $\Delta_1 + \Delta_2$ is restrained to be equal to 1/3 ; the other Ba positions in the crystal are obtained from the $\begin{pmatrix} 3 \\ t \end{pmatrix}$ symmetry operator. This model of modulation is illustrated in Fig. 1 for x=5/17 crystal. It explains correctly the satellite reflections and appears better than the model A (lowering of the reliability factors). As verified, the displacement $U_3(\overline{x}_{4,2})$ along c_2, $i.e.\ u_{0,z} \times c_2$ is negligible or very small within the three crystals, preserving the Ba interspace along **c**.

3.2.2 The $(Mn_{1-x}Na_x)O_3$ sublattice

Different models were also used to describe the Mn and Na atomic modulation.

Model I : a discontinuous atomic string In this model, chosen in previous related studies, the displacements along z of Na and Mn were described from sawtooth functions, with Δ_{Mn} and Δ_{Na} intervals ($\Delta_{Mn} + \Delta_{Na} = 1/2$), centred at $\overline{x}_{4,1} = 0$ and 1/4 respectively [31, 32] ; two additional harmonics were introduced for the Mn atom in order to better explain the 4D electron density map. Note that this model implies a perfect ordered sequence of Mn and Na atoms along [001]. Curves corresponding to the Mn and Na displacements, refined in this model, are shown in Fig. 2 for x=5/17.

Model II : a continuous atomic string This model used a single atom, the Mn atom, but an occupancy modulation is introduced to account for the existence of Na atoms in some unit cells ; moreover, harmonics (2 and 4) were considered to describe the U_z displacements. The odd harmonics are restrained to be equal to 0 owing to the high 4D symmetry $\begin{pmatrix} \overline{3} & m \\ \overline{1} & s \end{pmatrix}$ of the site. This harmonic model (the corresponding atomic string are drawn in Fig.2) was found better than the previous one (significant lowering of the agreement R factors).

As explained above, the crystal with $x \simeq 2/7$ was also refined using a classical 3D approach (R$\overline{3}$c SG). From the z coordinates thus obtained for the Mn atoms, an average position and atomic displacements along the z axis could be easily deduced and then the displacive modulation of this atom in the 4D approach is specified. As verified, these displacements fit better with the continuous model (model II) than with the discontinuous one (model I).

Concerning the crystal with γ =2/3 (commensurate structure) both a 3D refinement and a 4D refinement were carried out and compared. The different possible sections corresponding to the P3, P321 and P$\overline{3}$ 3D symmetries in physical space were tested within the 4D treatment. As expected, the best result is obtained for the section corresponding to the P321 3D SG. The model used to describe (Mn,Na) atoms combined both atomic displacement and occupancy modulation. Thus, atomic displacement parameters (ADP) modulation (thermal motion modulation) was not applied to these atoms to avoid correlations between the different modulation parameters.

The oxygen atom In the three crystals, the oxygen atom shows very large displacement amplitudes (up to 0.7 Å) along z; this effect is related to the insertion of Na atoms in metallic columns to form locally triangular prisms. A sawtooth function smoothed with two harmonics was used to account for the electron density map shown in Fig. 3.

3.2.3 Global procedure

Orthogonalization procedure [33] was used for O, Ba(1) and Ba(2) atoms defined on reduced Δ interval of $\overline{x}_4$ ($\Delta < 1$) to ensure a better convergence of the refined parameters. Modulation function for a parameter p of an atom μ, defined in a restricted Δ interval of $\overline{x}_4$ ($\Delta < 1$) is given by :

$$U_p^{\mu}(\overline{x}_4) = \sum_{n=0}^{m} U_{p,n}^{\mu} F_n^{\mu}(\overline{x}_4)$$

The $U_{p,n}^{\mu}$ terms are the Fourier terms describing modulation refined within the orthogonalisation procedure and m the number of harmonics used in the refinement. $\{F_n^{\mu}(\overline{x}_4)\}$ stands for a set of orthogonalized functions on the Δ interval (Schmidt procedure) ; each functions is written as :

$$F_i^{\mu}(\overline{x}_4) = B_{i,0}^{\mu} + \sum_{n=1}^{\underbrace{(i+1)/2}} A_{i,n}^{\mu} \sin 2\pi n\overline{x}_4 + \sum_{n=1}^{\underbrace{i/2}} B_{i,n}^{\mu} \cos 2\pi n\overline{x}_4$$

where the coefficients $B_{i,0}^{\mu}$, $A_{i,n}^{\mu}$ and $B_{i,n}^{\mu}$ are calculated during the refinement to ensure the orthogonalisation of the $F_n^{\mu}(\overline{x}_4)$ functions ; $\underbrace{(i+1)/2}$ and $\underbrace{i/2}$ mean integer part of (i+1)/2 and i/2 respectively.

Moreover, a modulation of the ADPs was considered for O and Ba atoms because their close atomic surroundings change significantly throughout the unit cells.

The refinement results of the three crystals are gathered in Table 2, 3 and 4.

4 Discussion

4.1 The octahedra-prisms sequence

Using the only result concerning the displacive modulation of Mn (or Na) atom (models I and II), it appears difficult to know for certain in which unit cells the Na atoms are located

(notably in the Mn-Na border zones, Fig 2). However, owing to a strong displacive modulation, oxygen lattice draws a framework of face sharing trigonal prisms (P) and octahedra (O) in which metallic atoms are inserted ; an accurate sequence of O and P polyhedra along z can be given. The heigth of the prisms (3.6 Å) and this of the octahedra (2.35 Å), roughly constant within both columns for the three studied compounds, allows us to determine without any doubt the location of metallic species. The height of the prism is, indeed, too large to accommodate Mn atoms. We conclude that the Mn atoms exhibit an octahedral coordination while the Na atoms are found inside trigonal prisms. The sequences of the MnO_6 octahedra and NaO_6 prisms, running along [001], are compared in Fig 4. The structure of the two crystals with $\gamma = 9/14$ and $\gamma = 11/17$ are visualized within the supercell (a,b,14c_1) and (a,b,17c_1) respectively. As expected, the O and P sequence along [001] is in agreement with the one foreseen for instance using the method summarized in our previous work [27] or the Farey-tree rule [34]. Thus, considering the crystal defined by x=2/7 in the supercell approximation (c=14c_1) ; x is written as $x = \frac{2}{7} = \frac{1}{4} \oplus \frac{1}{3} = \frac{0}{1} \oplus \frac{1}{3} \oplus \frac{1}{3}$ and the polyhedra sequence is derived from the juxtaposition of the sequences corresponding to $x = \frac{0}{1}$ (1O) and twice $x = \frac{1}{3}$ (2O-1P); the result then obtained 3O, 1P, 2O, 1P is that observed on the half period. The actual sequence $(3O,1P,2O,1P)_2$ is simply derived by using twice the previous sequence. Note that the two structural blocks are symmetry related through an horizontal two fold axis perpendicular to (1 0 0) (Fig. 5) yielding a 2_1 axis parallel to **c** within each atomic column. The (O) and (P) sequence of the crystal with x=5/17 is more complicated and can be written as (3O,1P,2O,1P,2O,1P,3O,1P,2O,1P).

4.2 The bonding scheme

The variations of the metal-oxygen (M-O) distances versus the internal parameter are shown in Fig 6a for the value x=5/17. For the two other compounds, the plots essentially keep the same shape and amplitudes. Accurate interatomic distances for the 3D treatment of x=1/3 composition are reported elsewhere [27]. In the Fig 6a, two sets of curves are drawn and compared, corresponding to the two proposed Mn-Na modulation models. As discussed below, even if model I (discontinuous) leads to more likely M-O distances (no "unrealistically" small Na-O distances ranging from 2.05 to 2.20 Å), R factors lowering is obtained by model II (continuous). Moreover, a careful examination of the 3D refinement, done for the crystal with x=2/7, intensifies our confidence on this model: indeed, the 4D atomic string calculated for Mn atoms from the supercell description shows a "zigzag" shape very similar to the continuous dark line drawn in Fig 2. These "unrealistic" distances calculated using the model I (continuous) for some unit cells are inevitably generated by the continuous change from short Mn-O distances to longer Na-O distances. But one should keep in mind that, according to the commensurate assumption, only discrete value of t yield true distances as detailed in the legend for Fig 6. One must also remind that the choice of model I or II does not change the whole model and more particularly does not affect the octahedra-prisms sequence. Indeed, the stacking sequence is rather imposed by the oxygen displacive modulation which is independent of the considered model. Then the use of the model I or II only changes the position of the metallic cation inside the polyhedron and, both models lead, *i*n globo to reasonable MnO and NaO environments.

Of course, a possible interpretation of the mismatch between "better" NaO environment obtained in the model I and the R lowering observed for the model II could be related to a slight static disorder in the cationic sites, *e*.g. due to a loss of coherence between columns or to the intergrowth with micro phases showing different x values. Moreover, this disordered aspect could appear reinforced by the observation of the Mn/Na occupancy curve (Fig 2), very different of the curve expected for the ordered model (saw tooth functions, model I). But once more, such discrepancies are inevitably generated by the continuous model that intrinsically shows a great flexibility to take into account disordered phenomena. Thus considering, the preferred model II, two types of distances can be clearly evidenced. The first one is typical of Mn-O bond lengths ranging from about 1.85 to 2.00 Å($\sigma \simeq 0.02$ Å) in the three crystals, while the second one is consistent with Na-O bond lengths : 2.02-2.72 Å(while the literature predict d_{Na-O} greater than 2.2 Å, see previous comments about "unrealistic" small distances in prisms). Within both octahedral and prismatic Mn/Na cations, the oxygen coordination is formed by two sets of three M-O distances with d_{M-O} range from 0 to 0.7 Åfor prisms and from 0 to 0.15 Åfor octahedra, depending on t. This observation pictures possible strong off-centering of cations inside their polyhedra along columns.

This bonding scheme leads, using the bond valence formalism [35], to an oxidation state of Mn higher than 4

(Fig 6b). This result is in agreement with the approximate oxidation state value of 4.5 implied by the chemical formula, *i*.e. +4.5 for x =1/3, +4.4 for x = 2/7 and +4.416 for x = 5/17. This "exotic" mixed valence for manganese in same crystallographic sites is discussed elsewhere [27], but briefly it is noteworthy that, to our knowledge, the only compound which exhibit this feature is the 6H-perovskite $Ba_3ErMn_2O_9$ [36], otherwise Mn^{4+} and Mn^{5+} being segregated in octahedral and tetrahedral environments [37], respectively. Within the Na prismatic coordination, since short Na-O distances on one side of the prism are balanced by longer ones on the other side, the bond valence calculation leads to an oxidation state close to 1.

The Fig 7 shows the M-$M^{(transl.001)}$ distances for the value x=5/17. Thus, running along the columns axis, Mn-Mn_{dimers}, Mn-$Mn_{trimers}$ Mn-Na and Na-Mn pairs are encountered. Mn-Mn bonds with minimum distances of 2.33 and 2.40 Å are observed in some unit cells of crystals γ=9/14 and γ=11/17 respectively, the maximum distance reaching 2.7 Å in the other unit cells. Therefore, in a general manner, it is noteworthy that intra-trimer Mn-Mn bonds are sensitively shorter than intra-dimer Mn-Mn bonds (in good agreement with results from the 3D x=1/3 refinement that solely contains dimers, *e*.g. 2.53(2) Å$< d_{Mn-Mn} <$2.66(2) Å). This result leads to imagine Mn-Mn interactions, *i*.e. metallic bonds in some unit cell and relaxation phenomena in the others , distributed differently for each unit cell and, of course driving the electric and magnetic properties of such materials. For (Mn-Na) distances, they are generally greater (up to 3.2 Å) but shorter (2.4 Å) also exist, as a consequence of the polyhedral off-centring.

The Ba atoms are bonded to oxygen atoms belonging to the three surrounding metallic columns. Concerning the Ba(2) atom, the most shifted from the special position x=1/3, the dispersion of the Ba-O distances is moderate (2.67 Å$\leq d \leq$ 2.95 Å); a ninefold or an eightfold coordination is then achieved for this Ba. The Ba-O distances relating to the other baryum type (Ba(1)) are more dispersed, ranging from 2.5 to 3.0 Å; this Ba atom exhibits three types of coordination 8, 9 and 10.

4.3 The twin phenomenon

The macroscopic twin element is a two fold axis of [001] direction. The refined volume ratios of the two variants are nearly equal to 1/2 for the crystals with x=2/7 and 5/17 (for the crystal with x=1/3, the twin volum ratio is 0.7/0.3), suggesting the existence of a strong binary pseudo symmetry of the structure. This property was verified from the study of the atomic positions in the supercells. A noteworthy pseudo symmetry, involving a [001] two fold screw axis passing through the origin, is observed for the crystal x=2/7 ; it should be noted that for each atom of coordinate z is associated an atom of coordinate 1/2+z owing to the R$\overline{3}$c symmetry of the structure approximant. The departure from the binary symmetry arises from small discrepancies on the x and y coordinates of Mn, Na and Ba atoms. The distance between the ideal positions, generated from the twin element, and the actual positions are about 0.1 Å for all the atomic pairs of oxygen and Ba atoms. In the crystal with x=5/17, the same twin element is found but the pseudo symmetry is less stressed mainly because the c mirror is no longer a symmetry element of the structure approximant.

5 Concluding remarks

Structures reported in this paper are in agreement with the previous studies, already cited above, on related compounds. The octahedra-prisms sequences observed are that foreseen by the Farey rule and the refined models are close to those published in the literature. However, the insertion of monovalent cations (Na^+) instead of divalent cations induces drastic changes in the $(A'_xB_{1-x})O_3$ framework. Thus, a strong dilatation of the trigonal prisms is evidenced ; the height of the prisms is about 3.6 Å in Na-based compounds against $\simeq$ 3 Å for $A_{1+x}(A'_xB_{1-x})O_3$ phases with a divalent A' cation. Moreover, exotic oxidation state (about 4.5) is stabilized for the Mn atoms ; this fact is discussed elsewhere [27].

Note that, an idealized structure following the stacking sequences given by the Farey tree should be in agreement with a model built up from discontinuous functions as crenel or sawtooth functions. Nevertheless, models finally chosen to describe the $Mn_{1-x}Na_xO_3$ framework of the the studied crystals used continuous harmonic functions. They seem to offer more flexibility to take into account possible disorder phenomena or stacking faults.

To conclude, classical 1D composite structures are built up from two interpenetrating sublattices exhibiting two independant periodicities along one direction. A modulation makes it possible the accommodation of the structural

mismatch resulting from the existence of these two periodicities. The case of $A_{1+x}(A'_xB_{1-x})O_3$ compounds appears very different. The x value imposes the periodicity on $A'_xB_{1-x}O_3$ sublattice and, as the A atoms are located only in the atomic planes $[A_3A'O_6]$ and $[A_3O_9]$ (see Introduction part), it induces also that of the A_{1+x} sublattice. This fact is illustrated by the expressions of the c_1 and c_2 parameters given in the introduction. Then, the octahedra-prisms sequence imposes the periodicity for the both sublattices which are, consequently, not any more independant. In the same way, since $\gamma = \frac{1+x}{2}$, the modulation is only related to the x value (and then to the P-O sequence) and not to the mismatch between the $A'_xB_{1-x}O_3$ and A_{1+x} sublattices. The commensurate or incommensurate character of the modulation depends of the rational or irrational value of x.

6 Supporting Information Available:

4D X-ray crystallographic files in JANA2000 format of the three compounds reported. This material is available free of charge via the Internet at http://pubs.acs.org.

References

[1] Campa, J., Gutierrez-Puebla, E., Monge, A., Rasines, I. & Ruiz-Jalero, C., J. Solid State Chem. (1994), 108, 230

[2] Abraham, F., Minaud, S., & Renard, C., J. Mater. Chem. (1994), 4, 1763

[3] Nguyen, T.N & zur Loye, H.C., J. Solid State Chem. (1995), 117, 300

[4] Nguyen, T.N, Lee, P.A. & zur Loye, H.C., J. Science (1996), 271, 489

[5] Campa, J., Gutierrez-Puebla, E., Monge, A., Rasines, I. & Ruiz-Jalero, C., J. Solid State Chem. (1996), 126, 27

[6] Battle, P.D., Blake, G.R., Darriet, J., Gore, J.G. & Weill, F., J. Mater. Chem. 7 (1997), 1559

[7] Battle, P.D., Blake, G.R., Sloan, J. & Vente, J.F., J. Solid State Chem. 136, (1998) 103

[8] Blake, G.R., Sloan, J., Vente, J.F.,& Battle, P.D., Chem. Mater 10 (1998), 3536

[9] El Abed, A., Gaudin, E., Lemaux, S., & Darriet, J., Solid State Sci. 3 (2001) 887

[10] El Abed, A., Gaudin, E., Darriet, J.& Whangbo, M.H., J. Solid State Chem. 163 (2002) 513

[11] El Abed, A., Gaudin, E., zur Loye, H. C. & Darriet, J., Solid State Sciences 5 (2003) 59

[12] Gourdon, O., Petříček, V., Dušek, M., Bezdicka, P., Durovic, S., Gyepesova, D. & Evain, M., Acta Crystallogr. B55 (1999), 841

[13] Stitzer, K. E., El Abed, A., Darriet, J., & zur Loye, H.C., J. Am. Chem. Soc. (2004), 126(3), 856

[14] Cussen, E.J., Vente, P.D. & Battle, J., J. Am. Chem. Soc. 121 (1999) 3958

[15] Dussarat, C., Fompeyrine, J. & Darriet, J., Eur. J. Solid State Inorg. Chem. (1995), 32, 3

[16] Stitzer, K.E., El Abed, A., Darriet, J. & zur Loye, H.C., J. Am. Chem. Soc. 123 (2001), 8790

[17] Hodeau, J.L., Tu, H.Y., Bordet, P., Fournier, T., Strobel, P., Marezio, M. & Chandrashekhar, G.V., Acta Crystallogr. B48 (1992), 1

[18] El Abed, A., Gaudin, E. & Darriet, J., Acta Crystallogr. (2002), C58, 138

[19] Ukei, K., Yamamoto, A. Watanabe, Y., Shishido, T. & Fukuda, T., Acta Crystallogr. (1993), B49, 67

[20] Onoda, M., Saeki, M., Yamamoto, A. & Kato, K., Acta Crystallogr. (1993), B49,929

[21] M. Evain, F. Boucher, O. Gourdin, V. Petříček, M. Dušek & P. Bezdicka, Chem. Mater. (1998) 10, 3068

[22] Perez-Mato, J.M., Zakhour-Nakhl, M., Weill, F. & Darriet, J., J. Mater. Chem. 9 (1999), 2795

[23] Zakhour-Nakhl, M., Weill, F., Darriet, J. & Perez-Mato, J.M., Int. J. Inorg. Mater. 2 (2000), 71

[24] Zakhour-Nakhl, M., Darriet, J., Claridge, J.B., zur Loye, H.C. & Perez-Mato, J.M., Int. J. Inorg. Mater. 2 (2000), 503

[25] Zakhour-Nakhl, M., Claridge, J.B., Darriet, J., Weill, F., zur Loye, H.C. & Perez-Mato, J.M., J. Am. Chem. Soc. 122 (2000), 1618

[26] El Abed, A., Elqebbaj, S.E., Zakhour, M., Campeaux, M., Perez-Mato, J.M. & Darriet, J., J. Solid State Chem. 161 (2001), 300

[27] Quarez, E., Roussel, P., Pérez, O., Leligny, H., Bendraoua, A. & Mentré, O., Solid State Sci. 6 (2004), 931

[28] Quarez, E., Ph. D thesis dissertation, University of Lille I, France, Oct. 2002

[29] Duisenberg, J.M., Kroon-Batenburg, M.J. & Schreurs, M.M., J. Appl. Cryst. (2003), 36, 220

[30] Petříček, V. & Dušek, M.(2000). Jana2000. The crystallographic computing system. Institute of Physics, Praha, Czech Republic.

[31] Petříček, V., Van der Lee, A. & Evain, M., Acta Crystallogr. (1995), A51, 529

[32] Boucher, F., Evain, M.& Petříček, V., Acta Crystallogr. (1996), B52, 100

[33] Janickis, V., Nečas, M., Novosad, J., Dušek, M. & Petříček, V., Acta Crystallogr. (2002), B58, 977

[34] Farey series of 1025, Royal Society Mathematical Tables, 1950, volume I, University Press Cambridge

[35] Brese, N.E. & O'Keefe, Acta Crystallogr. (1991), B47, 192

[36] Rabbow, C., & Mûller-Buchbaum, H., Z. Natursorsch., 49b, 1277 (1994)

[37] Floros, N., Michel, C., Hervieu, M., & Raveau, B., J. Solid State Chem. (2002), 168, 11

7 Figures

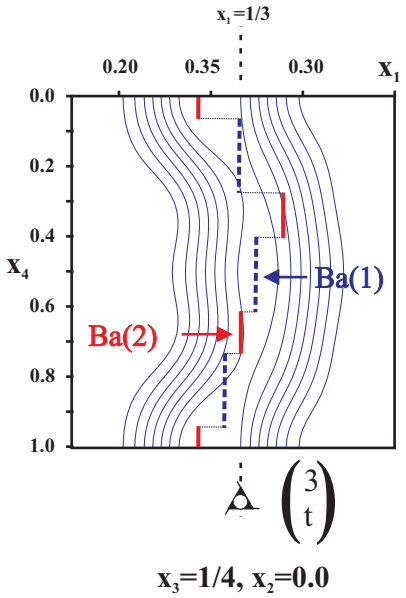

Figure 1: **Observed Fourier map around the baryum position. The dark and dark dashed lines correspond to the refined model B.**

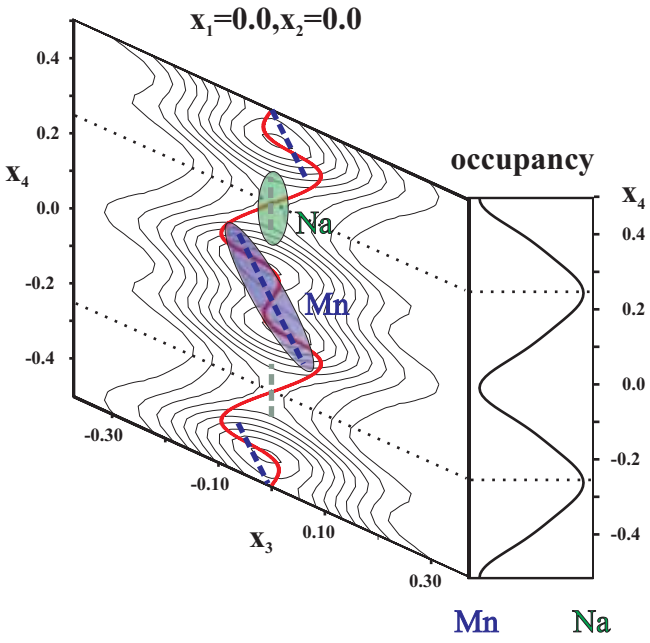

Figure 2: **Observed $x_3 - x_4$ Fourier map for the Mn and Na atoms (drawn for $Ba_{1+x}[Na_xMn_{1-x}O_3]$, x=5/17). The continuous dark line illustrates the harmonic model (model II, the selected one) while the grey dashed lines show the model I. The curve in the right part of the figure corresponds to the occupancy refined for Mn in model II.**

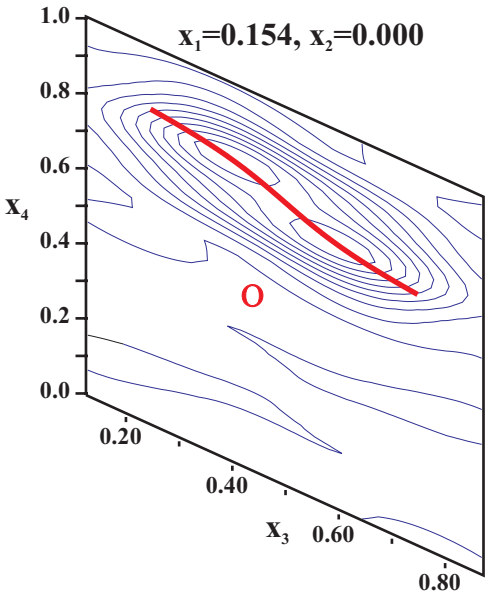

Figure 3: **Observed $x_3 - x_4$ Fourier map around the oxygen position (drawn for $Ba_{1+x}[Na_xMn_{1-x}O_3]$, x=5/17). The dark line shows the function used to describe the atomic string.**

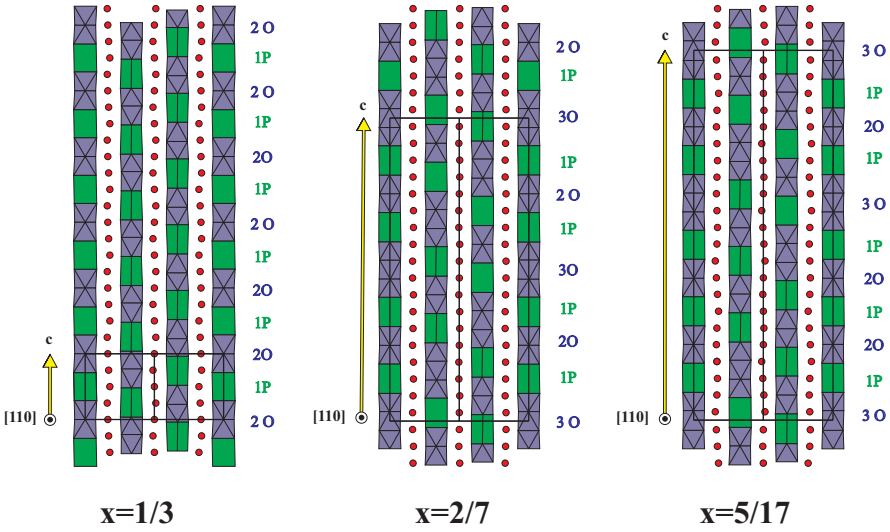

Figure 4: **Projection along [110] of the $Ba_{1+x}[Na_xMn_{1-x}O_3]$ structures for x=1/3, 2/7 and 5/17. The prisms NaO_6 (P) and the octahedron MnO_6 (O) are drawn in dark grey and light grey respectively ; Ba atoms are symbolized as grey circles. The polyhedra sequence is also indicated for each structure.**

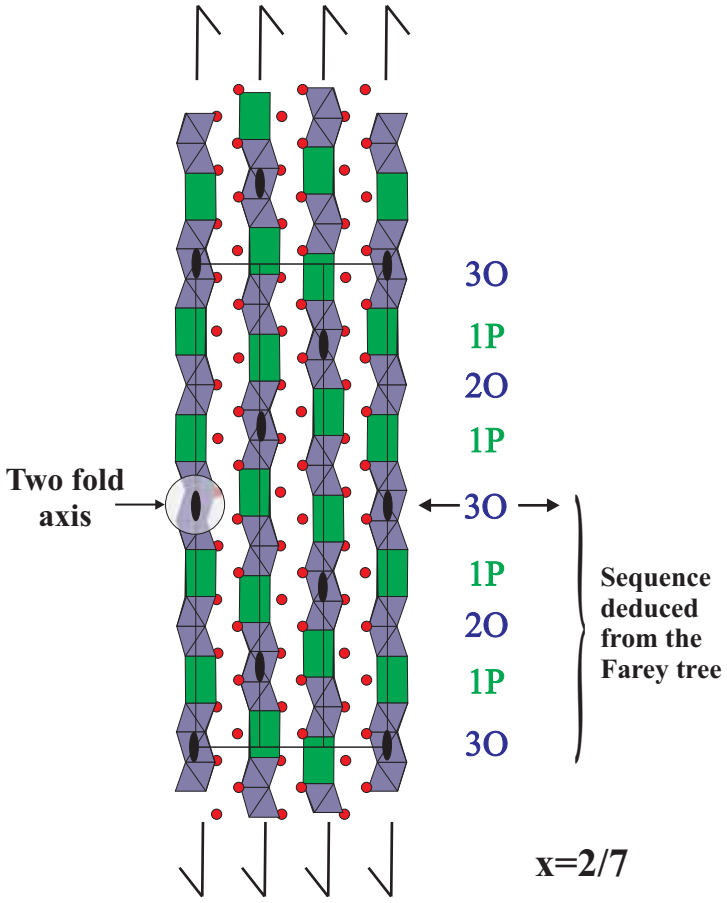

Figure 5: **Projection along [100] of the $Ba_{1+x}[Na_xMn_{1-x}O_3]$ structures with x=2/7. The Prism-Octahedron (O-P) sequence, indicated next to the structure, enlightens the role of the two fold axis in the periodicity along c. Note that the 2_1 axes parallel to c appears only inside each metallic column, not in the whole structure.**

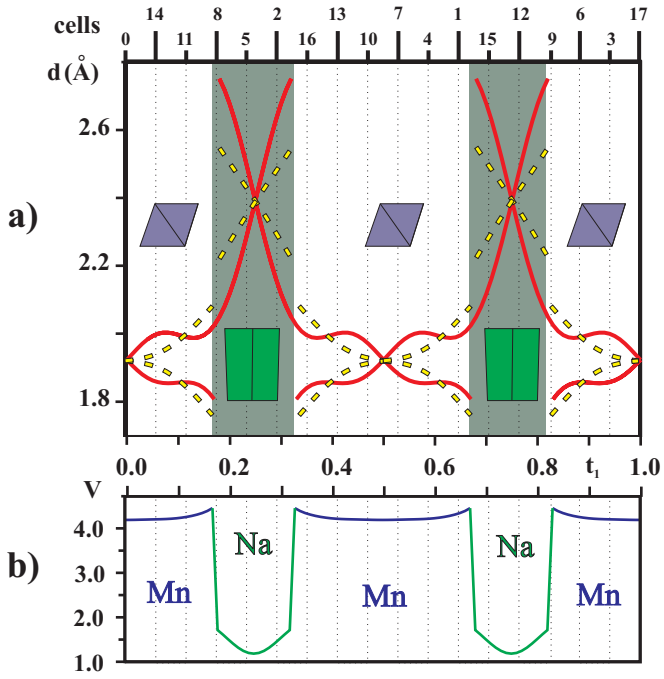

Figure 6: **a) Evolution of the metal-oxygen distances d (Å) versus t_1 in the harmonic continuous model (solid curves) and in the discontinuous model (dashed curves). These results correspond to the refinement of the crystal with x=5/17. The grey and white regions indicate the existence domains of NaO_6 prisms and of MnO_6 octahedra respectively. Vertical dotted lines are guide for eyes ; they help the reader to built the "17 cells" sequence (*i*.e. O-P sequence) corresponding to the supercell description (see Fig. 4c). b) Evolution of the metal valence versus t_1. Valence is minimum for metal in a prismatic coordination and maximun elsewhere.**

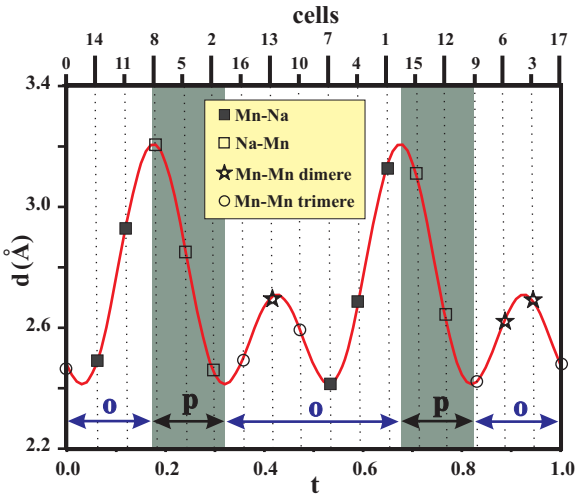

Figure 7: **Evolution of the metal-metal distances (Å) versus t_1 in the harmonic continuous model for the crystal with x=5/17. O and P refere to octahedron and prism respectively. Symbols correspond to distances effectively reached in the (a,b,17c) supercell.**

8 Tables

	$Ba_{1+x}[Na_xMn_{1-x}]O_3$		
x value	1/3	2/7	5/17
	Composite Approach		
	Sublattice 1 : $[Na_xMn_{1-x}]O_3$		
symmetry	Rhombohedral		
$a_1 = b_1$ (Å)	10.022(4)	10.006(5)	9.99(1)
c_1 (Å)	2.743(6)	2.698(4)	2.70(3)
	Sublattice 2 : Ba_{1+x}		
symmetry	Trigonal		
$a_2 = b_2$ (Å)	10.022(4)	10.006(5)	9.99(1)
c_2 (Å)	4.116(8)	4.197(3)	4.18(4)
$\gamma = \frac{c_1}{c_2}$	2/3	9/14	11/17
Super Space Group	$R\overline{3}m(00\gamma)0s$: $P\overline{3}c1(00\gamma^{-1})$		
	3 D Approach		
possible	$t = 0$, SG : P$\overline{3}$	$t = 0$, SG : R$\overline{3}c$	$t = 0$, SG : P$\overline{3}$
3D	$t = \frac{1}{36}$, SG : P32	$t = \frac{1}{28}$, SG : R$\overline{3}c$	$t = \frac{1}{204}$, SG : P32
sections	t, SG : P3	t, SG : R3c	t, SG : P3
	Supercell		
symmetry	Trigonal		
$a = b$ (Å)	10.022(4)	10.006(5)	9.99(1)
c (Å)	8.235(8)	37.77(4)	45.93(4)
wavelength (Å) / $(\sin\theta/\lambda)_{max}$	0.71073 / 0.9		
scan strategy	$\phi - \omega$		
scan angle (°)	1	0.6	0.3
Dx (mm)	34	70	70
unique reflections (I$\geq 3\sigma_1$)			
Main reflections	459	538	431
Satellites reflections 1^{st} order	538	936	822
Satellites reflections 2^{nd} order	-	247	347
Absorption correction	Gaussian integration based upon crystals morphology		
Internal R value (%)			
before correction	9.9	6.7	7.4
after correction	6.8	5.9	5.7
refinement program	JANA2000 [30]		
number of refinement parameters	50	52	61
weighting scheme	$1/\sigma_I^2$		
$\Delta\rho_{min}$ / $\Delta\rho_{max}$ ($\overline{e}$/Å^3)	3.22/3.92	4.46/1.62	3.06/2.89
F(000)	357	326	348
Reliability factors (R)	0.0430	0.0480	0.0560
Main reflections (R_0)	0.0450	0.0380	0.0575
Satellite reflections 1^{st} order (R_1)	0.0420	0.0530	0.0500
Satellite reflections 2^{nd} order (R_2)	-	0.1120	0.0770

Table 1: Details of data collection.

		$Ba_{1+x}[Na_xMn_{1-x}]O_3$		
x value		1/3	2/7	5/17
	x	$0^{\dagger}$	$0^{\dagger}$	$0^{\dagger}$
	y	$0^{\dagger}$	$0^{\dagger}$	$0^{\dagger}$
	z	$0^{\dagger}$	$0^{\dagger}$	$0^{\dagger}$
	$z\sin(2\pi\overline{x}_{4,1})$	-0.044(1)	-0.067(1)	-0.057(1)
Mn/Na	$z\sin(4\pi\overline{x}_{4,1})$	0.030(3)	0.067(3)	0.050(2)
	o	0.822(6)	0.713(4)	0.779(8)
	$o\cos(2\pi\overline{x}_{4,1})$	0.259(9)	0.183(6)	0.232(6)
	$o\cos(4\pi\overline{x}_{4,1})$	-0.04(2)	0.12(2)	0.016(12)
	$o\cos(6\pi\overline{x}_{4,1})$	$0^{\ddagger}$	0.06(3)	$0^{\ddagger}$
	x	0.154(6)	0.1541(4)	0.1541(4)
	y	$0^{\dagger}$	$0^{\dagger}$	$0^{\dagger}$
	z	$0.5^{\dagger}$	$0.5^{\dagger}$	$0.5^{\dagger}$
	$x\sin(2\pi\overline{x}_{4,1})$	0.0034(11)	0.0039(6)	0.0027(5)
	$x\cos(2\pi\overline{x}_{4,1})$	0.0026(3)	0.0014(3)	0.0017(3)
	$y\cos(2\pi\overline{x}_{4,1})$	0.0052(6)	0.0028(5)	0.0034(6)
	$z\cos(2\pi\overline{x}_{4,1})$	0.027(2)	0.017(2)	0.021(2)
	$x\sin(4\pi\overline{x}_{4,1})$	-0.0023(4)	-0.0020(4)	-0.0021(3)
O	$y\sin(4\pi\overline{x}_{4,1})$	-0.0045(8)	-0.0040(8)	-0.0041(6)
	$z\sin(4\pi\overline{x}_{4,1})$	-0.0157(4)	-0.012(3)	-0.005(2)
	$x\cos(4\pi\overline{x}_{4,1})$	-0.0018(16)	-0.0014(10)	-.0023(6)
	$u_{0,z}$	-0.278(3)	-0.281(2)	-0.272(3)
	$\overline{x}^0_{4,1}$	$0.75^{\ddagger}$	$0.75^{\ddagger}$	$0.75^{\ddagger}$
	Δ	$0.5^{\ddagger}$	$0.5^{\ddagger}$	$0.5^{\ddagger}$
	x	0.32404(9)	0.32690(6)	0.3256(1)
	y	$0^{\dagger}$	$0^{\dagger}$	$0^{\dagger}$
Ba(1)	z	$0.25^{\dagger}$	$0.25^{\dagger}$	$0.25^{\dagger}$
	$x\sin(2\pi\overline{x}_{4,1})$	-0.0049(1)	$0^{\ddagger}$	$0^{\ddagger}$
	$x\cos(2\pi\overline{x}_{4,1})$	-0.0099(2)	$0^{\ddagger}$	$0^{\ddagger}$
	$y\sin(2\pi\overline{x}_{4,1})$	-0.0027(2)	$0^{\ddagger}$	$0^{\ddagger}$
	$u_{0,z}$	$0^{\ddagger}$	$0^{\ddagger}$	-0.0067(10)
	$\overline{x}^0_{4,2}$	$0.5^{\ddagger}$	$0.5^{\ddagger}$	$0.5^{\ddagger}$
	Δ	0.20(1)	0.2430(9)	0.219(6)
	x	0.3626(2)	0.3574(2)	0.357(1)
	y	$0^{\dagger}$	$0^{\dagger}$	$0^{\dagger}$
Ba(2)	z	$0.25^{\dagger}$	$0.25^{\dagger}$	$0.25^{\dagger}$
	$x\cos(2\pi\overline{x}_{4,1})$	-0.0051(3)	$0^{\ddagger}$	$0^{\ddagger}$
	$u_{0,z}$	$0^{\ddagger}$	$0^{\ddagger}$	$0^{\ddagger}$
	$\overline{x}^0_{4,2}$	$0^{\ddagger}$	$0^{\ddagger}$	$0^{\ddagger}$
	Δ	0.13(1)	0.0903(9)	0.114(6)

Table 2: Refinement results : Occupancy and position (average and modulated) parameters. Only modulated parameters relevant at least for one of the three compounds are printed. † fixed by symmetry. ‡ fixed because the deviation to the noted value is not significant.

	F_0	=	$B_{0,0}$	1.000
	F_1	=	$B_{1,0}$	2.069
		+	$A_{1,1}$	3.249
O	F_2	=	$B_{2,1}$	1.414
	F_3	=	$B_{3,1}$	2.271
		+	$A_{3,2}$	2.675
	F_4	=	$B_{4,0}$	2.187
		+	$A_{4,1}$	2.785
		+	$A_{4,3}$	1.953
	F_0	=	$B_{0,0}$	1.000
	F_1	=	$A_{1,1}$	2.947
Ba(1)	F_2	=	$B_{2,0}$	1.348
		+	$B_{2,3}$	2.553
	F_0	=	$B_{0,0}$	1.000
	F_1	=	$A_{1,1}$	4.049
Ba(2)	F_2	=	$B_{2,0}$	-1.553
		+	$B_{2,4}$	2.749

Table 3: Orthogonalized functions. See part 3.2.3 for notations.

		$Ba_{1+x}[Na_xMn_{1-x}]O_3$		
x value		1/3	2/7	5/17
	β_{11}	0.0072(6)	0.0058(3)	0.022(3)
Mn	β_{22}	0.0072(6)	0.0058(3)	0.038(5)
	β_{33}	0.0204(12)	0.0262(9)	0.032(5)
	β_{12}	0.0036(3)	0.0029(2)	0.019(3)
	β_{11}	0.019(2)	0.0120(10)	0.022(3)
	β_{22}	0.022(3)	0.0159(14)	0.038(5)
	β_{33}	0.023(3)	0.0249(15)	0.032(5)
	β_{12}	0.011(1)	0.0079(7)	0.019(3)
O	$\beta_{11}\sin(2\pi\overline{x}_{4,1})$	0.014(2)	0.004(1)	0.005(1)
	$\beta_{22}\sin(2\pi\overline{x}_{4,1})$	0.010(3)	0.005(2)	0.008(2)
	$\beta_{33}\sin(2\pi\overline{x}_{4,1})$	0.004(3)	0.007(2)	0.006(2)
	$\beta_{11}\cos(2\pi\overline{x}_{4,1})$	0.005(2)	0.0023(8)	0.0038(9)
	$\beta_{13}\cos(2\pi\overline{x}_{4,1})$	-0.0045(14)	-0.0047(10)	-0.003(1)
	β_{11}	0.0145(5)	0.0217(3)	0.0226(4)
	β_{22}	0.0272(7)	0.0294(4)	0.0324(5)
	β_{33}	0.0186(7)	0.0187(4)	0.0201(4)
	β_{12}	0.0136(4)	0.0147(2)	0.0116(2)
	β_{13}	0.0014(2)	0.0038(2)	0.0032(1)
	β_{23}	0.0029(4)	0.0075(3)	0.0064(2)
	$\beta_{11}\sin(2\pi\overline{x}_{4,1})$	-	-0.0033(4)	-0.0033(4)
Ba(1)	$\beta_{11}\cos(2\pi\overline{x}_{4,1})$	-	-0.0033(4)	-0.0033(4)
	$\beta_{22}\cos(2\pi\overline{x}_{4,1})$	-	-	0.0006(5)
	$\beta_{12}\sin(2\pi\overline{x}_{4,1})$	-	-	-0.005(1)
	$\beta_{13}\sin(2\pi\overline{x}_{4,1})$	-	-	-0.0041(15)
	$\beta_{23}\sin(2\pi\overline{x}_{4,1})$	-	0.0108(5)	0.0083(10)
	$\beta_{12}\cos(2\pi\overline{x}_{4,1})$	-	-	-0.0021(7)
	$\beta_{13}\cos(2\pi\overline{x}_{4,1})$	-	0.0012(3)	0.0028(6)
	$\beta_{23}\cos(2\pi\overline{x}_{4,1})$	-	0.0025(7)	0.0056(12)
	β_{11}	0.006(5)	0.0031(4)	0.0074(4)
	β_{22}	0.008(1)	0.0037(4)	0.0087(5)
	β_{33}	0.003(1)	0.0159(5)	0.0164(5)
	β_{12}	0.0041(5)	0.0018(2)	0.0044(3)
	β_{13}	-0.0025(4)	-0.0023(2)	-0.0019(1)
Ba(2)	β_{23}	-0.005(1)	-0.0046(3)	-0.0037(3)
	$\beta_{11}\sin(2\pi\overline{x}_{4,1})$	-	-	-0.0061(10)
	$\beta_{11}\cos(2\pi\overline{x}_{4,1})$	-	-	-.0061(10)
	$\beta_{12}\sin(2\pi\overline{x}_{4,1})$	-	-	-0.0019(9)
	$\beta_{13}\sin(2\pi\overline{x}_{4,1})$	-	-	-0.003(2)
	$\beta_{12}\cos(2\pi\overline{x}_{4,1})$	-	-	-0.002(1)

Table 4: Refinement results : Atomic displacement (average and modulated) parameters.Only modulated parameters relevant at least for one of the three compounds are printed. - fixed to zero because not significant.